Quantum vortex sheets

M. H. Chang,[1] T. Chiueh,[1,2,*] and C. R. Lo[1]
[1]*Physics Department, National Central University, Chung-Li, Taiwan*
[2]*Physics Department, National Taiwan University, Taipei, Taiwan*
(Received 9 June 1998)

Vortex sheets can be viable defects present in quantum systems. In two dimensions, the vortex sheet is represented by a line connecting a pair of branch points of half-integer phase rotation. A stationary vortex sheet can exist in a finite system either with a pinning potential or without any pinning potential as long as the rotational symmetry is broken. Despite the rotational symmetry breaking, an angular-momentum-like quantum number is always required for the existence of a stationary vortex sheet. Such a property is closely related to the integrability of a dynamical system. [S1063-651X(98)10012-0]

PACS number(s): 47.15.Hg, 67.20.+k, 67.57.Fg

I. INTRODUCTION

Topological defects in ordered systems are present on all scales, from the microscopic [1–4], mesoscopic [4–7], to macroscopic [8,9] scales. Line defects in three dimensions (or point defects in two dimensions) are the most commonly studied objects in microscopic scales. Such a defect pertains to a singular line around which the displacement, velocity, or polarization vector rotates by an integral multiple of 2π along any path in space. This singular line is often called the vortex line. In a crystalline solid, vortex lines often manifest themselves as dislocations [1,4,6]. In type-II superconductors [2,3], vortex lines are the sites at which the magnetic fields are allowed to penetrate, and play the central role in limiting the superconductivity in the presence of high fields. However, in mesoscopic and macroscopic scales, other types of defects are often present and have received much attention. Noticeably, in liquid crystals, a variety of different defects have been classified and studied in detail. These defects are generally called textures [5]. Textures and defects are dynamically caused by the symmetry-breaking effects during phase transitions. Even in high-temperature field theory, their existence has also been predicted during the cosmological phase transitions in the early universe [10].

On the microscopic level, except for the quantum vortex lines, few studies have been directed to addressing the general existence of quantum textures. Recently, the fluid formulation of quantum dynamics has been examined and it is concluded that without dissipation, the topological defects are bound to be frozen in the quantum fluid, much like those in the ideal classical fluid, and can preserve their integrity throughout the evolution [11]. An interesting texture is the vortex sheet in three dimensions. The sheet can be better described in two dimensions as a branch line. This line connects a pair of branch points of half-integer phase rotation; the counterpart of such a quantum vortex sheet in liquid crystals has been observed and studied in details [4–6]. In the present work, we will further elaborate on the existence and structures of the quantum vortex sheets. Particularly, we will show that their existence is closely linked to the existence of an angular-momentum-like quantum number as well as the integrability of a dynamical system.

Section II gives the mathematical formulation of a particular type of stationary vortex sheet which has a zero energy and is infinitely extended in the third dimension. The boundary condition is described in Sec. III. Two examples of the zero-energy vortex-sheet solutions are numerically solved and given in Sec. IV. Although these solutions can exist in a system with boundaries of arbitrary shape, their existence in fact requires specifically tailored external potential wells, present at the sheets, in order to pin the quantum particles. In Sec. V, we discuss the natures of vortex sheets and explore the possibilities of other stationary vortex-sheet solutions in the absence of pinning potentials.

II. ZERO-ENERGY VORTEX SHEETS

The Schrodinger equation reads

$$-\frac{\hbar^2}{2m}\nabla^2\psi(\mathbf{r})+V(\mathbf{r})\psi(\mathbf{r})=E\psi(\mathbf{r}). \tag{1}$$

Consider the situation where $E=0$ and the potential $V(\mathbf{r})\neq 0$ only in some finite volume. It follows that in the region where $V(\mathbf{r})=0$, we have

$$\nabla^2\psi(\mathbf{r})=0, \tag{2}$$

and in the region where $V(\mathbf{r})\neq 0$ we have

$$\nabla^2\psi(\mathbf{r})=\frac{2mV(\mathbf{r})}{\hbar^2}\psi(\mathbf{r}). \tag{3}$$

For the cases that are of interest to us, the potential V is nonzero only within an infinitely thin sheet, which is to be identified as the vortex sheet. In other regions, Eq. (2) prevails and it is no more than the Laplace equation, which must be supplemented by a set of suitable boundary conditions to yield viable solutions.

In the present work, the vortex sheet is assumed to be infinitely extended and has no structure in the third dimen-

*Electronic address: chiuehth@phys.ntu.edu.tw

sion and we consider only its spatial structure in two dimensions. To construct the vortex-sheet solution, we first express the solution as

$$\psi(\mathbf{r}) = \exp\{a[\phi_1(\mathbf{r}) \pm i\phi_2(\mathbf{r})]\}, \tag{4}$$

with the real functions ϕ_1 and ϕ_2, respectively, characterizing the amplitude and phase of the complex wave function ψ, and a is a constant. Demanding $\psi(\mathbf{r})$ to be a single-valued function, we find that the constant a must be chosen so that $a\phi_2(\mathbf{r})$ becomes an anglelike periodic function around the two-dimensional Euclidean space.

It follows from Eq. (2) that

$$\nabla^2\phi_1(\mathbf{r}) = 0 \tag{5}$$

and

$$\nabla^2\phi_2(\mathbf{r}) = 0. \tag{6}$$

If we further demand that

$$\nabla\phi_1 \cdot \nabla\phi_2 = 0, \tag{7}$$

i.e., the orthogonal families of $\phi_1 = \text{const}$ and $\phi_2 = \text{const}$, the functions ϕ_1 and ϕ_2 become conjugate functions in the theory of complex variables. It is therefore sufficient only to solve for, e.g., $\phi_1(\mathbf{r})$, from which $\phi_2(\mathbf{r})$ trivially follows by virtue of the Cauchy-Riemann equations:

$$\frac{\partial\phi_1}{\partial y} = -\frac{\partial\phi_2}{\partial x}, \quad \frac{\partial\phi_1}{\partial x} = \frac{\partial\phi_2}{\partial y}. \tag{8}$$

Of particular interest among the two conjugate functions is the phase function ϕ_2, where $a\hbar\nabla\phi_2$ can be identified as an irrotational velocity field of the quantum particle. As $a\phi_2$ should be an anglelike variable, we find that $\nabla\times\nabla\phi_2 = \mathbf{0}$ except at the vortex sheets where Eq. (2) breaks down. That is, ϕ_2 is a multivalued function with a singular line located at an infinitely thin vortex sheet.

III. BOUNDARY CONDITIONS

For an isolated vortex sheet, we would like to have a solution where the density $e^{2a\phi_1} \to 0$ and current $ae^{2a\phi_1}\nabla\phi_2 \to 0$ as $r \to \infty$. In practice, both density and current can only decay algebraically slowly for the zero-eigenvalue state. Hence for any solution that obeys the form given by Eq. (4), we can only place the numerical boundary as remote as the computational memory allows, so remote that the probability density can decay by several orders of magnitude from the vortex sheet. However, such a solution is still not an exact solution due to its failure in exactly satisfying the boundary condition. Nevertheless, it is possible to circumvent this boundary problem if one gives up the functional form required by Eq. (4) for the eigenfunction. Our strategy in dealing with the boundary problem involves a suitable linear combination of the trial solutions of Eq. (5) given by two different ''trial'' potentials V. The composite solution can be made to satisfy the desired boundary condition at the walls; moreover, once the composite solution is solved, the actual pinning potential V_n can also be self-consistently determined in terms of the two trial potentials V.

To be specific, we let the boundary assume a constant finite ϕ_1 for the trial solutions, so that $\nabla\phi_1$ is always normal to the boundary walls, implying that $\nabla\phi_2$ is always parallel to the boundary walls. This completes the prescription of the outer boundary condition for the trial solutions. On the other hand, for a stationary vortex sheet the velocity field $\nabla\phi_2$ must be parallel to the vortex sheet; otherwise, the vortex sheet would be advected around by the self-induced velocity field and a stationary state would not be possible. Consequently, much like the boundary walls discussed above, the inner boundary, i.e., the vortex sheet, must assume a constant value $\phi_1 = \phi_0$.

Combining Eqs. (2) and (3), we find that the problem of solving for the trial solution is identical to an equivalent problem of solving for the electric potential given by a charged sheet, with an unknown surface charge density that equals $2mV(\mathbf{r})/a\hbar^2$, i.e.,

$$\nabla^2\phi_1 = \frac{2mV(\mathbf{r})}{a\hbar^2}. \tag{9}$$

Poisson's equation now replaces the Laplace equation, Eq. (5). In addition, since the amplitude of the wave function is arbitrary, we may arbitrarily choose a nonzero value for ϕ_0.

What remains unknown is the functional form of $V(\mathbf{r})$ on the sheet. This problem is now reduced to an equivalent problem where one seeks the charge distribution on a perfectly conducting sheet surrounded by a perfectly conducting box of a different electric potential. The charge distribution can be determined only after the electric potential around the conducting sheet has been determined. That is, one may fix the functional form of $V(\mathbf{r})$ only after one has solved for the trial function ϕ_1. The phase ϕ_2 can also be easily constructed once ϕ_1 is determined by using Eq. (8).

IV. NUMERICAL SOLUTIONS

We may numerically solve for the electric potential given by a perfectly conducting sheet of any arbitrary shape with the proper boundary conditions discussed above. We adopt the relaxation method to solve Poisson's equation. A fictitious time dependence is introduced to Poisson's equation so that it becomes a diffusion equation:

$$\frac{\partial\phi_1}{\partial t} - \nabla^2\phi_1 = 0, \tag{10}$$

where the source term at the vortex sheet has been incorporated as the boundary condition, which sustains a constant electric potential $\phi_1 = \phi_0$ at the sheet.

A. Planar vortex sheet

The computation is carried out in a square box with 500×500 grid points. The vortex sheet is located in the middle of the box 50 grids long and one grid wide. We choose the boundary wall to be also a conducting wall which is an equipotential surface with another arbitrary value $\phi_1 = \phi_0'$.

A standard stable numerical scheme is adopted to solve the diffusion equation. Independent of the initial conditions,

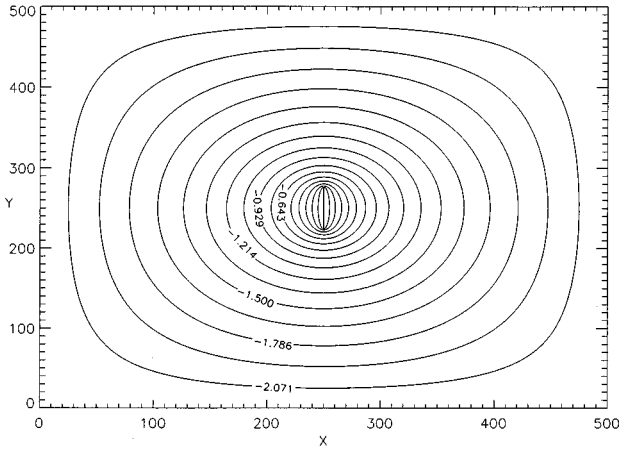

FIG. 1. Contour plot of the trial function $a\phi_1$ for the planar vortex sheet. The actual velocity field has a magnitude equal to $\hbar|a\nabla\phi_1|$ and its direction is along the contour either clockwise or anticlockwise. The spatial coordinate is in an arbitrary unit.

the solution of Eq. (10) always settles to a unique stationary state. The stationary solution ϕ_1 has no node. Depicted in Fig. 1 is the contour plot of the resulting solution $a\phi_1(\mathbf{r})$. Along the constant-ϕ_1 contours are the flow lines of the velocity field ($a\nabla\phi_2$), whose magnitude is the same as $a|\nabla\phi_1|$ according to the Cauchy-Riemann equations, and whose sense of rotation can be arbitrary. In order for ψ to be a single-valued function, the phase $a\phi_2$ must be quantized. Quantization of $a\phi_2$ can be achieved by choosing a proper value for a. We may fix this proper value of a by integrating $a|\nabla\phi_1|$ along any constant-ϕ_1 contour, so that the closed-contour integral of $\int a|\nabla\phi_1|dl$ assumes $\pm 2l\pi$, where l is an integer. The above contour integral has made use of the equality $|\nabla\phi_1|=|\nabla\phi_2|$. When l assumes integers other than unity, the probability density will become the $2l$th power of that with $l=1$ and it decays outward more rapidly. Once a is fixed, the trial potential $V(\mathbf{r})$ can be derived from Gauss' law by examining the amount of flux $a\nabla\phi_1$ emerging from the sheet locally. The resulting $2mV(\mathbf{r})/\hbar^2$ along the sheet, for $l=1$, is shown in Fig. 2. When l assumes other integers, the

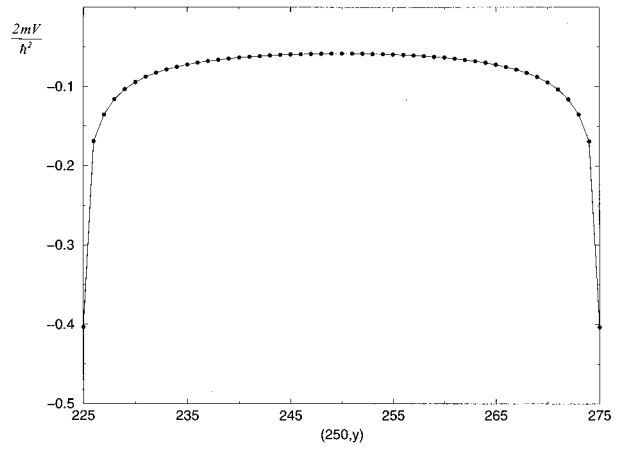

FIG. 2. Pinning potential $2mV/\hbar^2$ of the trial function ϕ_1 shown in Fig. 1. The pinning potential $2mV_n/\hbar^2$ of the actual solution is greater than $2mV/\hbar^2$ by a factor 1.016.

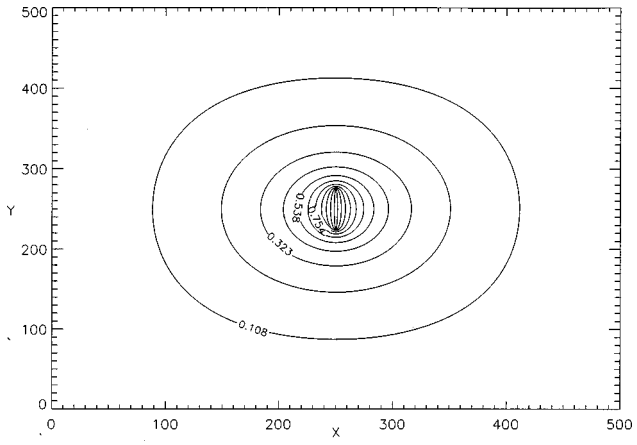

FIG. 3. Contour plot of the actual wave-function amplitude, $|\psi|$, for the planar vortex sheet.

quantum potential will need to be enhanced by l times.

In a finite system, a proper solution can be constructed, where ψ vanishes at the system boundary, by the following manipulations. We find that the proper wave function can be expressed as a linear combination of the trial functions solved above,

$$\psi=[e^{a\phi_1}-\beta e^{-a\phi_1}]e^{\pm ia\phi_2}, \tag{11}$$

instead of Eq. (4), where β is a constant. Except for the yet-to-be-determined pinning potential at the sheet, this combination is a solution to $\nabla^2\psi=0$. Now, choose $\beta=e^{2a\phi_0'}$. At the boundary $\phi_1=\phi_0'$, such a solution can indeed satisfy the boundary condition that $\psi=0$ and hence is the proper solution. The resulting amplitude of this wave function is shown in Fig. 3. Unlike the vortex line, at which the probability density must vanish due to the infinitely large velocity ($\propto r^{-1}$) at the line [12], the quantum particle has the largest probability at the vortex sheet. In addition, since the phase $a\phi_2$ remains the same for this proper wave function, the actual velocity field is the same as that derived from the test function ϕ_1 given in Fig. 1.

The velocity field, proportional to the gradient of ϕ_1 in Fig. 1, is strongest around the edges of the vortex sheet, since the incompressible flow must make sharp turns near the edges. The associated centrifugal forces are larger than elsewhere and hence it requires a deeper potential well at the edge to pin the flow. In fact, the strength of vorticity in the sheet is closely related to $V(\mathbf{r})$ shown in Fig. 2. Using Eq. (8), we find $\nabla^2\phi_1\hat{\mathbf{z}}=\nabla\times\nabla\phi_2$, and using Eq. (9), we find the vorticity $a\nabla\times\nabla\phi_2=2mV\hat{\mathbf{z}}/\hbar^2$.

The equivalence to $a\phi_1$ of Eq. (4) for the proper wave function, i.e., $\ln[\exp(a\phi_1)-\exp(a(2\phi_0'-\phi_1))]$, is no longer the analytical conjugate of the phase $a\phi_2$, and hence the Cauchy-Riemann equations do not apply to them. Furthermore, the actual quantum potential must change accordingly to reflect the new combination for the wave function. In fact, due to the choice of combination given in Eq. (11), the two trial potentials V of the two trial solutions have similar profiles although their signs and magnitudes are different. The actual potential V_n can be expressed in terms of the trial potential V depicted in Fig. 2 as

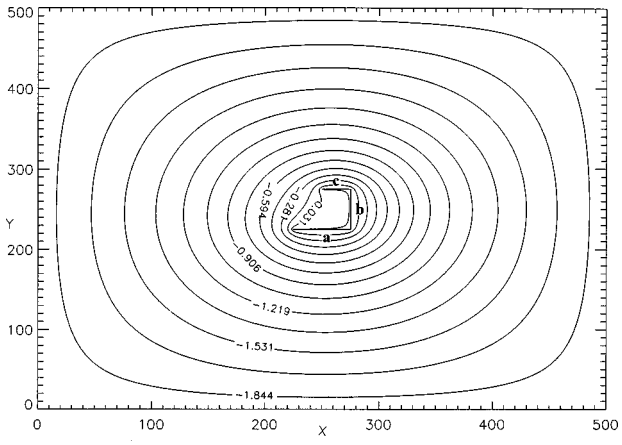

FIG. 4. Contour plot of the trial function, $a\phi_1$, for the L-shaped vortex sheet.

$$V_n(\mathbf{r}) = V(\mathbf{r})\left(\frac{1+\beta e^{-2a\phi_0}}{1-\beta e^{-2a\phi_0}}\right), \tag{12}$$

with $\beta = \exp[2a\phi_0']$. This result is straightforwardly obtained by applying Gauss' law to Eq. (11). It follows that to yield a solution that satisfies the proper boundary condition one needs the ratio $V_n/V > 1$ which approaches unity when $a(\phi_0 - \phi_0') \gg 1$. For the present case, we determine that $V_n/V = 1.016$.

The vortex-sheet state is in fact an excited state, since a proper linear combination of the two oppositely rotating degenerate states reveals a nodal line in it. We may adopt the V_n given above to determine its ground state numerically. The ground state has an amplitude peaking at where the potential well is deep near the two edges, and the ground-state eigenvalue is found to be $E = -3\times10^{-3}\hbar^2/m$ as opposed to $E = 0$ for the vortex-sheet state.

B. Distorted vortex sheet

We use the same computational configuration as the previous one, except that the vortex sheet is now distorted in an L shape. The same relaxation method and boundary conditions are employed to solve for the solution of Eq. (9). The resulting trial solution ϕ_1 for $l = 1$ is shown in Fig. 4; the trial potential associated with this trial solution, $2mV(\mathbf{r})/\hbar^2$ (also for $l = 1$), along each side (labeled by 1 and 2 in Fig. 4) of the vortex sheet is shown in Fig. 5. The actual potential V_n is found to be greater than V by a factor 1.28. For such a potential, the vortex-sheet state is also an excited state. We may also numerically determine the ground state. It has a higher probability amplitude near where the potential well is deep, and its eigenvalue is $E = -1.4\times10^{-3}\hbar^2/m$.

Revealed in Fig. 4 is also the velocity field induced by the vortex sheet along the contours. In the concave side of the sheet, the flow is distinctly weaker than the convex side of the sheet since the former has a shorter distance to travel than the latter. Again, the largest velocity field occurs near the edges of the sheet; in addition, immediately exterior to the L-shaped corner there is contained a larger velocity field. Near these locations the quantum potential well must be deeper in order to balance the enhanced centrifugal forces. This expectation is consistent with Fig. 5.

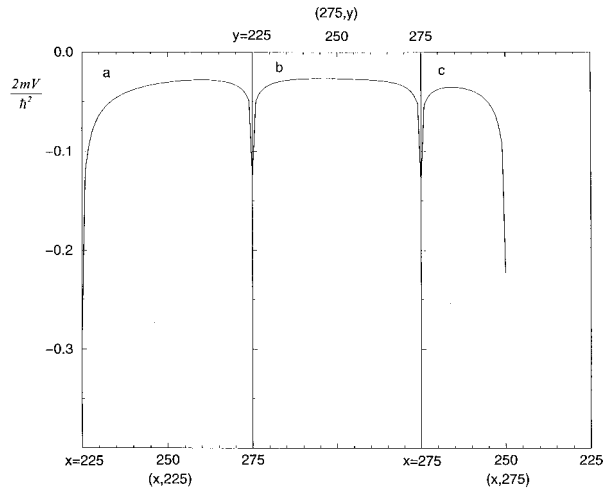

FIG. 5. Pinning potential $2mV/\hbar^2$ along each side (labeled by a, b, and c in Fig. 4) of the L-shaped vortex sheet. The ratio V_n/V equals 1.28.

V. DISCUSSIONS

In sum, we have obtained a particular type of stationary vortex-sheet solution, which is an excited state and which has a high probability density at the sheet due to the pinning of a quantum potential well at the sheet. Being an excited state is not a problem for the existence of quantum vortex sheet in nature since a Fermi gas can often occupy excited states. The major problem for it is that to yield a stationary wave function, the pinning potential well V must be fine-tuned in order to guide the velocity along the sheet. Such a fine-tuning does not seem able to arise either naturally or artificially in most physical systems. Hence, a quantum vortex sheet may seem most likely to be nonstationary, advected by the self-induced velocity governed by Biot-Savart's law. For such a transient state, no specific pinning quantum potential is required. If it is indeed so, the quantum vortex sheet would probably not be so interesting nor would it deserve much attention. However, as will be elaborated below, without any pinning potential there are possibilities for the existence of stationary vortex-sheet states, much like the line vortex states. Recall from Eq. (11) that the wave function can be expressed as a linear combination of trial solutions. We may adjust the value of β in such a way that $\beta = -e^{2a\phi_0}$. The wave-function amplitude has the property that $\nabla(\exp[a\phi_1] + \exp[-a\phi_1]) = 0$ at $\phi_1 = \phi_0$; that is, the probability density is a smooth function across the vortex sheet. From Eq. (12), the singular quantum potential V must vanish accordingly. However, such a stationary vortex-sheet solution does not satisfy the proper boundary condition of a finite-size system where $\psi = 0$ at the boundary. This difficulty is due primarily to our assumption of a vanishing eigenenergy E in Eq. (2). When we relax the condition $E = 0$, stationary vortex-sheet solutions can actually arise in the absence of pinning potentials, provided that suitable boundaries are given.

A natural coordinate for describing a planar vortex sheet is the elliptic coordinate (ξ_1, ξ_2), where x

$=d\cosh(\xi_1)\cos(\xi_2)$ and $y=d\sinh(\xi_1)\sin(\xi_2)$, or $x+iy=2d\cosh(\xi_1+i\xi_2)$. The coordinates $\xi_1(x,y)$ and $\xi_2(x,y)$ are conjugate functions, and the constant-ξ_1 contours in the x-y plane trace confocal ellipses, whose focal points are separated by a distance $2d$ on the x axis. On the other hand, the coordinate ξ_2 is similar to the angularlike variable $a\phi_2$ constructed earlier, which changes by $\pm 2l\pi$ around a closed loop. The two-dimensional Helmholtz equation can be transformed into [13]

$$\frac{\partial^2\psi}{\partial\xi_1^2}+\frac{\partial^2\psi}{\partial\xi_2^2}+k^2d^2[\cosh^2(\xi_1)-\cos^2(\xi_2)]\psi=0 \qquad (13)$$

in terms of the elliptic coordinate, where k^2 is the eigenvalue equal to $2mE/\hbar^2$ for our quantum-mechanical problem. This equation is separable. Let $\psi=f(\xi_1)g(\xi_2)$, and one finds that Eq. (13) becomes

$$\frac{d^2f}{d\xi_1^2}+[k^2d^2\cosh^2(\xi_1)-l^2]f=0 \qquad (14)$$

and

$$\frac{d^2g}{d\xi_2^2}+[l^2-k^2d^2\cos^2(\xi_2)]g=0, \qquad (15)$$

where l^2 is a separation constant related to a generalized angular momentum. Note that Eq. (15) is the Mathieu equation, to which Floquet's theorem applies. When the boundary is remotely located, one may consider the low-energy states. In the low-k^2d^2 (or low-$2mEd^2/\hbar^2$) limit, we can ignore $k^2d^2\cos^2(\xi_2)$ in Eq. (15), which then yields a solution $g(\xi_2)=\exp(\pm il\xi_2)$ with l being an integer. On the other hand, the term $k^2d^2\cosh^2(\xi_1)$ in Eq. (14) can never be ignored, in spite of the smallness of k^2d^2 due to its association with the large factor $\cosh^2(\xi_1)$ at large ξ_1.

For any given integer l, Eq. (14) can be solved with the boundary condition that $df/d\xi_1=0$ at $\xi_1=0$. When $\xi_1<\ln(2l/kd)$, the solution is approximately $f\approx\cosh(l\xi_1)$. However, as soon as $\xi_1>\ln(2l/kd)$, the solution f will begin to oscillate and the oscillation amplitude decreases with the distance ξ_1 as $e^{-\xi_1/2}$, which becomes $r^{-1/2}$ in terms of the radial distance r in the cylindrical coordinate. At large distances, the wave function ψ resembles $J_l(kr)e^{il\theta}$ given by a point vortex of angular momentum $l\hbar$. Such a *free* vortex sheet solution requires only a small positive eigenenergy, although it can never be a ground state.

If the system has a finite size L, the eigenvalue k^2 must assume a set of discrete values, the lowest of which is on the order of L^{-2}. However, for such an eigensolution to exist, the boundary must have a proper shape, i.e., an oval shape whose focal points will be those of the constant-ξ_1 contours. If not, it will be impossible for the wave functions to possess a generalized angular momentum as its quantum number, and the stationary quantum vortex sheet will be impossible in the absence of a pinning potential. Even when the system boundary is located at a very remote distance so that the system may seem to be boundary-free, the occurrence of such ''free'' vortex sheets in fact arises primarily from the focusing by a remote oval boundary.

The above change of coordinate employs a conformal transformation. We may proceed to employ the conformal transformation to examine another type of stationary vortex-sheet solution. Instead of using the elliptic coordinate, we may adopt the parabolic coordinate, (χ_1,χ_2), where $x+iy=(1/2)(\chi_1+i\chi_2)^2$. The constant-$\chi_1$ curves trace a family of confocal parabolas, $\chi_1\equiv[\sqrt{x^2+y^2}+x]^{1/2}$, where $\chi_1=0$ describes a half-line running from the origin $r=0$ to $r=\infty$ along the negative x axis. This half-line is exactly the branch line associated with a half-infinitely extended vortex sheet. Similar kinds of defects have been observed in the two-dimensional nematics of liquid crystals and are called the wedge disclinations [5]. The conjugate variable $\chi_2[\equiv\pm(\sqrt{x^2+y^2}-x)^{1/2}]$ runs from $-\infty$ to ∞, which corresponds to the polar angle from $-\pi$ to π.

The Helmholtz equation can be written as [13]

$$\frac{\partial^2\psi}{\partial\chi_1^2}+\frac{\partial^2\psi}{\partial\chi_2^2}+(\chi_1^2+\chi_2^2)k^2\psi=0, \qquad (16)$$

where k^2 is again proportional to the energy eigenvalue. This equation is also separable. The viable solution must satisfy $\partial\psi/\partial(\chi_1)^2=0$ at $\chi_1=0$ in order for it to be a smooth function there without any pinning potential. A close scrutiny shows that the only solution that can satisfy such a condition is the one with the separation constant l^2 equal to zero. Let $\psi=f(\chi_1)g(\chi_2)$. It follows that f satisfies the equation

$$\frac{d^2f}{d\chi_1^2}+k^2\chi_1^2f=0, \qquad (17)$$

and g also satisfies the same equation. Near $\chi_1=0$, we have an even solution, $f=c_0+c_4k^2\chi_1^4[1+O(\chi_1^2)]$, which meets the desired boundary condition. Asymptotically, $f\rightarrow|\chi_1|^{-1/2}\cos(k\chi_1^2+\theta)$ at large distances, where θ is a phase factor. On the other hand, near $\chi_2=0$, we have $g=\{c_0'+[1+O(k^2\chi_2^4)]\}\pm i\{c_1'\sqrt{k}\chi_2[1+O(k^2\chi_2^4)]\}$. Apparently, there is a net ''momentum'' flux ($\propto\mathrm{Im}[g^*(dg/d\chi_2)]$) around $\chi_2=0$, therefore supporting a rotational motion. In addition, the asymptotic behavior of g goes as $g\sim|\chi_2|^{-1/2}\exp[\pm ik\chi_2^2]$ at large distances. The $\pm$ signs are found to be attached to the two branches of the same solution on either side of the $\chi_1=0$ half-line. The vortex sheet is thus clearly demonstrated in this asymptotic expression near $\chi_1=0$, where $g\sim|x|^{1/4}\exp[\pm ikx]$. Such a vortex sheet can also arise from the focusing by a parabolic boundary, no matter how remote the boundary is located. The boundary reflects an incident particle from the lower/upper half-plane back to infinity along the upper/lower half-plane.

It should be stressed that the elliptic and parabolic coordinates are the only two nontrivial coordinates, besides the trivial polar and planar coordinates, that allow for separation of variables for the two-dimensional Helmholtz equation [13]. Since energy must be a quantum number and since the existence of stationary vortex sheets also requires an angular-momentum-like quantum number, it follows that separability, or integrability, of the Hamiltonian should be a necessary condition for the quantum vortex sheets to exist. In some cases, the quantum numbers must assume some specific values in order for the Hamiltonian to become integrable. Ex-

amples include the vortex sheets pinned by arbitrary-shaped singular potentials, for which the eigenenergy E must be zero. For these cases, the Hamiltonian is generally not integrable, and the vortex-sheet states correspond to the quasi-isolating integral hypersurfaces in classical mechanics [14]. Indeed, the Hamilton-Jacobi equation has a separable solution at the vortex-sheet state and the corresponding classical trajectories lie on a two-dimensional surface in the four-dimensional phase space. This singular integral surface in fact pertains to the invariant surface of Kolmogorov [15], Arnold [16], and Moser [17] type, the KAM surface. Such an invariant surface traces the separatrix which describes the trajectories of the barely bound particles attracted by the pinning potential.

As mentioned earlier, textures that exhibit finite and half-infinite vortex sheets have been observed in the nematics of liquid crystals. In view of the close analogy between the nematics and the superconductivity at the phase transition [5], we speculate that the quantum vortex-sheet defects may also be present, as bosonic excitations, in many-electron systems and may play a non-negligible role in determining the macroscopic physical properties of the condensed matters.

ACKNOWLEDGMENTS

This work is supported in part by the National Science Council of Taiwan under Grant Nos. NSC87-2112-M-008-009 and NSC87-2112-M-008-010.

[1] M. S. Seul and C. A. Murray, Science **262**, 558 (1993).
[2] J. Schelten, H. Ullmaier, and G. Lippmann, Z. Phys. **253**, 219 (1972).
[3] D. R. Nelson, Phys. Rev. Lett. **60**, 1973 (1988).
[4] P. M. Chaikin and T. C. Lubensky, *Principles of Condensed Matter Physics* (Cambridge University Press, Cambridge, 1995).
[5] P. G. de Gennes and J. Prost, *The Physics of Liquid Crystals* (Oxford University Press, Oxford, 1993).
[6] R. B. Meyer, Philos. Mag. **27**, 405 (1973).
[7] C. H. Chiang and Lin I, Phys. Rev. Lett. **77**, 647 (1996).
[8] C. A. Murray and R. A. Wenk, Phys. Rev. Lett. **62**, 1663 (1989).
[9] C. A. Murray, W. O. Sprenger, and R. A. Wenk, Phys. Rev. B **42**, 688 (1990).
[10] N. Turok, Phys. Rev. Lett. **24**, 2625 (1989).
[11] T. Chiueh, Phys. Rev. E **57**, 4150 (1998).
[12] P. A. M. Dirac, Proc. R. Soc. London, Ser. A **133**, 60 (1931).
[13] P. M. Morse and H. Feshbach, *Methods of Theoretical Physics* (McGraw-Hill, New York, 1953), Vol. 1, Chap. 5.
[14] G. Contopoulos, Astrophys. J. **68**, 1 (1963).
[15] A. N. Kolmogorov, Dokl. Akad. Nauk SSSR **98**, 527 (1954).
[16] V. I. Arnold, Usp. Mat. Nauk **18**, 13 (1963).
[17] J. Moser, in *Nonlinear Problems*, edited by R. E. Langer (University of Wisconsin Press, Madison, 1963), p. 139.